

Dynamical Signatures of Self-Phase-Locking in a Triply Resonant Optical Parametric Oscillator

Jean-Jacques Zondy* and Dmitri Kolker†

BNM-SYRTE, Observatoire de Paris, 61 Avenue de l'Observatoire, F-75014 Paris, France

Franco N. C. Wong

Research Laboratory of Electronics, Massachusetts Institute of Technology, Cambridge, Massachusetts 02139, USA

(Received 6 February 2004; published 21 July 2004)

We report on specific signatures of self-phase-locking in a cw frequency divide-by-three optical parametric oscillator subject to two competing $\chi^{(2)}$ nonlinear processes that couple the signal and idler subharmonic waves. The self-phase-locked pair appears as a broad fringe dip within the mode-pair cluster. We have also observed Hopf instabilities of the zero-detuning case at $\sim 4\times$ the pump threshold. These results open the path to experimental investigation of quantum entanglement and phase-locked transverse mode structures in this novel class of parametric oscillators.

DOI: 10.1103/PhysRevLett.93.043902

PACS numbers: 42.65.Yj, 42.65.Ky, 42.65.Sf

Self-injection-locking in optical parametric oscillators (OPOs) has attracted interest in recent years for studying the static and dynamical behavior of a highly nonlinear optical system and for its potential applications in precision frequency metrology, quantum information technology, and dissipative spatial structures. An OPO is a simple nonlinear quantum optical device that is well understood and characterized, and it is the workhorse for generating squeezed states of light and quantum entanglement. Unlike a conventional OPO, a self-phase-locked OPO (SPL-OPO) includes an additional mechanism to induce injection locking of the parametrically generated waves, thereby leading to a remarkable feature: The usual signal-idler phase diffusion is frozen, thus providing a more robust feedback control compared with the typical electronic feedback. Simple passive phase-locking mechanisms can be implemented only in a special class of OPOs: The subharmonic divide-by- n or n -to-1 OPOs, in which the pump frequency is related to the signal and idler frequencies by an integer relation ($n = 2, 3, 4$). Another remarkable feature of SPL-OPOs is the existence of n stable phase states, equally spaced by $2\pi/n$, associated with the *same* output intensity, thus allowing both phase and intensity encoding of information.

In a type-I (with copolarized outputs) 2-to-1 OPO, self-phase-locking occurs spontaneously when the parametric down-conversion is tuned to signal-idler degeneracy ($\omega_{s,i} = \omega$). However, operating a type-I OPO near degeneracy is extremely unstable [1]. A more stable type-II 2-to-1 SPL-OPO that contained an intracavity quarter-wave plate (QWP) for coupling the orthogonally polarized signal and idler subharmonic waves was first demonstrated by Mason and Wong [2]. The QWP orientation controls the *linear* coupling strength and allows strong, weak, and even zero signal-idler coupling. Static behavior such as thresholds and locking ranges of the two phase states were observed, but no details of the dynamical

features were studied. The 2-to-1 SPL-OPO thus provides convenient and stable optical frequency division for optical frequency measurements and synthesis. The quantum theory of a 2-to-1 SPL triply resonant OPO (SPL-TRO) has been recently studied in detail [3]. It was shown that self-phase-locking leads to various types of quantum correlations between photon numbers and the two associated phase states, and that continuous-variable (CV) entanglement can be realized for both nondissipative and dissipative dynamics in the entire range of input pump intensity. The same 2-to-1 SPL-OPO has also been recently utilized as a compact source for generating ultra-stable Einstein-Podolsky-Rosen entanglement and quadrature squeezing that extends to low baseband frequencies below 100 kHz [4]. In addition, it has been theoretically studied for its spatiotemporal dynamics and pattern formation [5].

The use of optical frequency division for generating multioctave frequency markers leads naturally to a divide-by-three (3-to-1) SPL-OPO [6]. In this system, the mechanism triggering self-injection locking of the two nondegenerate subharmonic waves is *nonlinear* [via an $\omega + \omega \rightarrow 2\omega$ second-harmonic generation (SHG) section of length L_2 in cascade with the $3\omega \rightarrow 2\omega + \omega$ OPO section of length L_1 , Fig. 1(a)]. More interestingly, a system with multiple nonlinearities has been proposed to generate continuous-variable multipartite quantum entanglement [7] that is of interest in advanced quantum information processing (quantum communication and computation). Although the quantum aspects of this 3-to-1 system remains to be studied in detail, together with the role of the phase stabilizing effect of a self-injection locked OPO, a 3-to-1 OPO divider with self-phase-locking may play a significant role in implementing higher-order quantum entanglement. In this Letter, we report on the first observation of the dynamical behavior of 3-to-1 SPL-TRO induced by two competing nonlinearities (Fig. 2, inset).

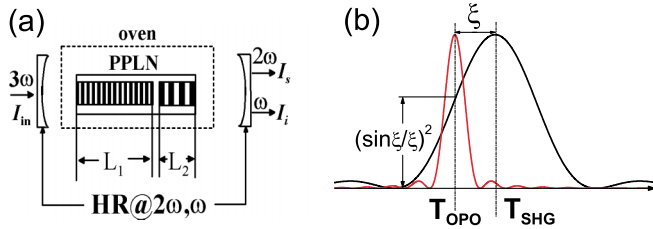


FIG. 1 (color online). (a) Schematic of the 3-to-1 SPL-TRO with a dual-grating temperature-tuned PPLN chip. (b) Tuning curves of the OPO and SHG processes versus temperature, showing the SHG phase mismatch $\xi = \frac{1}{2}\Delta k_{\text{SHG}}L_2$. The nonlinear coupling strength is controlled by $|\chi| \propto (L_2/L_1)|\text{sinc}(\xi)|$.

The static and dynamical behavior of the 3-to-1 SPL-OPO is far richer than that in the 2-to-1 system [8,9]. A striking feature of the 3-to-1 SPL-TRO is the predicted transition from subcriticality to supercriticality when the subharmonic waves oscillate with vanishing cavity detuning $\Delta_{s,i} \propto \omega_{s,i} - \omega_{\text{cav}}^{s,i} \rightarrow 0$ [8]. A critically slowed-down dynamics of the zero-detuning case is then predicted by the exact (full propagation) solutions of the cavity equations [8]. When the round-trip fractional loss of the idler exceeds the signal's ($\kappa_i > \kappa_s$), the steady-state intensities $I_{s,i}$ exhibiting phase tristability destabilize via a Hopf bifurcation at a modest input pump parameter $N = I_{\text{in}}/I_{\text{th}}$ defined as the ratio of the input photon intensity to the threshold intensity $I_{\text{th}} = \kappa_p^2 \kappa_s \kappa_i$. Figure 2, plotting the normalized phase-locked idler intensity $|\chi|^2 I_\omega$ versus N [curve (a)] as compared with the corresponding curve (b) for a conventional TRO ($L_2 = 0$), summarizes the expected dynamical signatures of the self-phase-locked pair (SPL pair). A prominent intensity dip should be observed at 3-to-1 division when the SHG competing process is active. Moreover, as a consequence of the critical slowing down, the Hopf instabilities whose threshold I_H increases with the pump round-trip amplitude reflectivity $r_p = 1 - \kappa_p$ are characterized by long periods of the order of tens of the idler photon mean

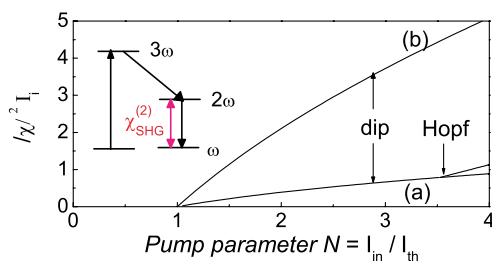


FIG. 2 (color online). Inset: Energy-level scheme showing the competing nonlinearities in the 3-to-1 SPL-OPO. Main frame: (a) Bifurcation diagram of the SPL-TRO idler intensity for $\Delta_{p,s,i} = 0$ versus the pump parameter N , as compared to a conventional TRO (b). The period of the Hopf instability is $58t_i$ at $N_H = 3.53$ and $64t_i$ at $N = 4$. The parameters are $\kappa_i = 0.0015$, $\kappa_s = 0.001$, $r_p = 0.75$, and $\chi = S = 0.2$.

cavity lifetime $t_i = \tau \mathcal{F}_i / \pi = \tau / \kappa_i$, where \mathcal{F} is the finesse and τ the cavity round-trip time [8,9]. For typical values $\tau \sim 1$ ns, $\mathcal{F}_i > 600$, and the loss parameters in Fig. 2, periodic instabilities in the kHz domain are expected while the predicted—but never observed due to its high threshold—Hopf instability in a conventional TRO have frequencies in the tens of MHz [10]. Such high-frequency Hopf instabilities were, however, reported in a pulsed implementation of the internally pumped OPO, another class of OPO subject to two competing nonlinearities [11].

The dual-section nonlinear medium sketched in Fig. 1(a) can be readily realized in periodically poled lithium niobate (PPLN) [12]. The ratio L_2/L_1 controls the strength of the nonlinear coupling when both $\chi^{(2)}$ processes are simultaneously type-I (*eee*) quasi-phase-matched at the same PPLN temperature $T = T_{\text{OPO}}$. Maximum coupling is given by the gain ratio of the two competing processes, $S \propto \chi_{\text{SHG}}^{(2)} L_2 / \chi_{\text{OPO}}^{(2)} L_1 \sim (L_2/L_1) / \sqrt{3}$ [8]. The control of the nonlinear coupling strength is far more subtle than in the linearly coupled type-II 2-to-1 SPL-OPO. Because both OPO and SHG processes are first-order quasi-phase-matched and temperature tuned, residual uncertainties in the dual-grating PPLN periods $\Lambda_{\text{OPO}} \simeq 28.85 \mu\text{m}$ and $\Lambda_{\text{SHG}} \simeq 34.75 \mu\text{m}$ may lead to the situation sketched in Fig. 1(b) in which the two gain curves are shifted by $\xi = \frac{1}{2}\Delta k_{\text{SHG}}L_2$ ($\Delta k_{\text{SHG}} = k_{2\omega} - 2k_\omega - 2\pi/\Lambda_{\text{SHG}}$ is the SHG phase mismatch [12]), and the field coupling strength $\chi = S \exp(i\xi) \sin\xi/\xi$ is reduced [7]. Fortunately, for a short enough SHG section, the SHG phase-matching bandwidth is $\sim 5\times$ broader ($\Delta T \sim 20^\circ\text{C}$) than the OPO gain bandwidth, thus increasing the overlap probability of both tuning curves at a given temperature T_{OPO} near the 3-to-1 point [8]. Perfect overlap requires in our case the selection of a specific pump wavelength $\lambda_p \sim 844.5$ nm, as fulfilled in this experiment.

Our SPL-TRO experimental setup is sketched in Fig. 3. The pump laser is a cw single-frequency ($\Delta\nu_p = 100$ kHz) master-oscillator power-amplifier (MOPA) AlGaAs semiconductor laser system [13,14] that is tunable around the wavelength $\lambda_p \simeq 844.5$ nm that minimizes ξ (Fig. 1). The MOPA can deliver up to $P = 430$ mW, about $N = 4$ times the measured TRO threshold

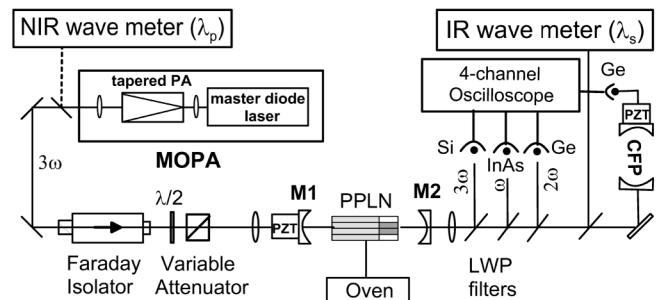


FIG. 3. Experimental setup.

($P_{th} \approx 100$ mW). The maximum total subharmonic output power is $P_s + P_i \approx 3.5$ mW. The nonlinear crystal is a type-I (*eee*), temperature-controlled (± 10 mK) dual-section PPLN with OPO-SHG section lengths $L_1 = 20$ mm and $L_2 = 10$ mm, which yields $S = 0.2$ with nominal room-temperature periods $\Lambda_{OPO} = 28.9$ μm , $\Lambda_{SHG} = 34.8$ μm for 3-to-1 phase matching of signal ($\lambda_s \sim 1267$ nm) and idler ($\lambda_i \sim 2533$ nm) at temperatures $132^\circ\text{C} < T < 136^\circ\text{C}$ [12]. The input-output facets are triple-band antireflection-coated (AR). The single-pass intensity loss $\epsilon_{s,i} \approx 2\kappa_{s,i}$ at $\omega, 2\omega$ was measured with the help of a previous PPLN-OPO [13] using a sensitive differential method, yielding $\epsilon_{s,i} < 0.5\%$ with a higher AR loss at ω dominating over the dual-band high-reflectance (HR) mirror loss ($R_{s,i} > 99.95\%$). We, hence, infer that the resonator loss corresponds to the case $\kappa_i > \kappa_s$. The outer PPLN gratings (Fig. 3) contain a single OPO section to allow for a straightforward comparison of the dynamics with and without the SHG section.

The OPO linear cavity is made of two meniscuses with radii-of-curvature $R = 5$ cm spaced by $L_{cav} \approx 11$ cm (quasiconcentric cavity, with optical path length $L_{opt} \approx 10$ cm), and the pump waist $w_p = 70$ μm at the center of the OPO section. Both mirrors partially transmit the pump, yielding a finesse $\mathcal{F}_p \approx 6$. We estimate the cavity finessses at ω and 2ω to be $\mathcal{F}_{s,i} > 600$. One of the mirrors is attached to a PZT ceramic tube for cavity-length scanning using a 20-Hz triangular voltage ramp to observe the cluster of mode pairs within the broad pump resonance fringe. A side-of-fringe locking servo is used to stabilize the oscillation on a single signal-idler mode pair in order to measure the signal wavelength using a ± 500 MHz accuracy IR-wave meter [14]. The 3-to-1 operating point ($\lambda_s = 3\lambda_p/2$) is then searched by tuning the PPLN temperature. Three different photodiodes with specific interference filters are used to monitor the output pump, signal, and idler intensities. To provide a diagnosis of self-phase-frequency locking, part of the signal wave is sent to a high-finesse ($\mathcal{F}_{CFP} = 360$, fringe linewidth ~ 1 MHz) confocal Fabry-Pérot etalon (CFP) that acts as a phase-frequency discriminator when it is voltage biased to transmit the signal frequency while the OPO cavity length is dithered. The CFP is made of a silica spacer of length $L_{CFP} = 20$ cm: Its free spectral range (FSR) $\Delta\nu_{CFP} = c/4L_{CFP} = 375$ MHz is, hence, a submultiple of the OPO cavity FSR $\Delta\nu_{OPO} \approx c/2L_{opt} = 1500$ MHz ($\Delta\nu_{OPO}/\Delta\nu_{CFP} \approx 4$). Adjacent mode pairs should then be simultaneously resonant for the same bias voltage of the CFP, owing to the FSR degeneracy.

The TRO cluster is observed on the positive ($\Delta L_{cav}/\Delta t > 0$) side of the triangular ramp, thus avoiding the slight cluster broadening effect due to optothermal self-stabilization of the optical path length on the negative side [14] that could hinder the observation of the expected intensity dip of the SPL pair. The pump, signal, idler, and biased CFP transmission are synchronously recorded by a digital oscilloscope triggered by the

ramp. Figure 4 shows the signal intensity dip observed in the cluster when the PPLN temperature is finely tuned around $T = 135^\circ\text{C}$ which corresponds to a measured $\lambda_s \approx 3\lambda_p/2$. The dip position within the cluster can be moved with tiny adjustments of the PPLN temperature ($\Delta T \leq 0.1^\circ\text{C}$), but disappears beyond this limit due to the finite width of the pump resonance. The dip is never observed when the TRO operates with the OPO-only grating (which yields a dense unresolved cluster [13]). We should point out that, in a singly resonant SPL-OPO, a peak instead of a dip is predicted [9].

While consecutive non-SPL pair jumps occur over a typical scan length with $\Delta L_{cav} \sim 1$ nm [13,14], the frequencies of the SPL pair do not change for $\Delta L_{cav} \sim 45$ nm as witnessed also by the clamped pump intensity. The calibration of the locking range is provided by the comparison of the CFP fringe width for a non-SPL pair (resulting in a sharp 1 MHz-wide fringe) with respect to the broad CFP fringe depicted in Fig. 4. In static operation, the TRO can remain stably on the SPL pair for several minutes without any cavity servo, while non-SPL pairs are subject to frequent mode hops (note that their half-fringe pattern with a sharp onset at $\Delta_{s,i} = 0$ is due to a delayed bifurcation phenomenon under the adiabatic detuning sweep). The bell-shaped SPL fringe in Fig. 4(a) results from detunings $\Delta_{s,i}(t)$ that vary according to the cavity eigenmode frequencies $\omega_{cav}^{s,i}(t)$. Such a bistable shape, with intensity increasing with the detuning, was predicted in Ref. [8]. Figure 4(b) displays a much flatter SPL transmission—which exhibits the widest locking range ($\Delta\nu_{lock} = 54$ MHz)—corresponding to a different bias voltage applied to the OPO cavity. This bias setting yields cavity eigenmode frequencies ($\omega_{cav}^s, \omega_{cav}^i$) that are closest to the 3-to-1 point which is solely

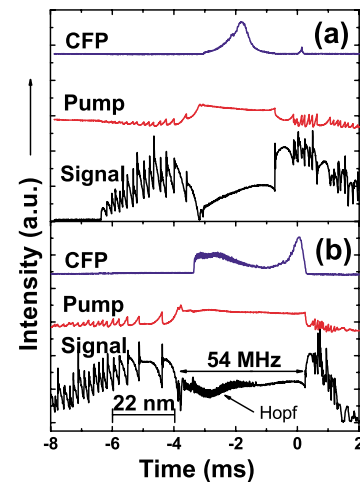


FIG. 4 (color online). Synchronous time traces of the signal, pump ($\lambda_p = 844.57$ nm) and CFP transmission (the latter being voltage biased to transmit the SPL signal wave). The pump power is $P = 420$ mW. The scale in nanometers gives the OPO cavity-length change during the scan. Different OPO cavity biases are applied for (a) and (b) (see text).

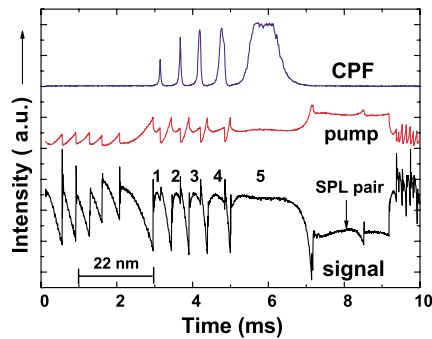


FIG. 5 (color online). Same as Fig. 4, except that the CFP is now resonant with the adjacent pairs (1–5) preceding the SPL pair.

determined by the pump frequency. In general, the SPL fringe shape depends on how close the cavity mode is relative to the divide-by-three point. We note that when the CFP is set to resonance with the SPL fringe it does not transmit the non-SPL mode pairs, suggesting a phase-pulling effect of the cavity mode nearest to the 3-to-1 point. This phase pulling is due to the additional nonlinear phase shift arising from the competing $\chi_{\text{OPO}}^{(2)}\chi_{\text{SHG}}^{(2)}$ interactions.

Only for a flat SPL fringe and for sufficiently strong pumping ($P \geq 400$ mW), small-amplitude (up to 5%) temporally periodic and sustained oscillations emerge during the scan as evident in the signal and CFP traces in Fig. 4(b). The self-pulsing frequency measured under static cavity length is extremely low ($f_{\text{Hopf}} \sim 20$ kHz, i.e., $\sim (70t_i)^{-1}$) as theoretically predicted in Fig. 2 with parameters close to the experimental values. These slow sinusoidal (for $\xi \approx 0$) instabilities correspond to the zero-detuning Hopf instabilities, since the $\Delta_{s,i} \neq 0$ Hopf bifurcation occurs at a much higher pump or detuning thresholds, with frequencies of the order of the inverse photon lifetime [8]. This slow dynamics results from the critical slowing-down phenomenon. A detailed study of these Hopf instabilities, whose wave forms and periods vary with ξ , will be given in a forthcoming paper.

Figure 5 shows the case when the CFP is made to transmit the adjacent pairs preceding the SPL pair. While all five adjacent modes are transmitted during the scan (the progressive decay is due to the residual mismatch of the OPO and CFP FSRs), the SPL pair is *not* transmitted due to the phase-pulling effect. The short interruption of the dipped fringe in its middle is not a mode jump but is caused by an out-and-in locking on the same SPL pair. In some traces, one could observe up to two such events in the dip, suggesting that these are jumps among the three phase states of the system which share the same intensity state. Indeed, setting the CFP to resonance with the dip, either one or the other part is transmitted but not both simultaneously. Finally, let us notice that the broadening of the fringes (1–5) next to the SPL fringe is an indication that complex $\chi_{\text{OPO}}^{(2)}\chi_{\text{SHG}}^{(2)}$

cascading processes occur away from the 3-to-1 point, self-injecting a number of adjacent mode pairs. We have verified this interpretation by a spectral analysis of these broadened modes with a short nondegenerate $\Delta\nu_{\text{FP}} = 150$ GHz Fabry-Pérot analyzer, with the evidence that up to 5 to 6 mode pairs are simultaneously oscillating. This observation opens up the prospect of a passively mode-locked operation of the detuned 3-to-1 SPL-OPO, if cavity dispersion can be compensated.

In conclusion, we have observed unambiguous signatures of self-phase-locking in a 3-to-1 SPL-TRO subject to two competing nonlinearities, in the form of a broad intensity dip at exact 3-to-1 division. We attribute the observed temporal dynamics to the Hopf instabilities of the zero cavity detuning oscillation. As compared with a complex electronically phase-locked 3-to-1 OPO divider [6,13], the cluster dip signature provides a convenient diagnosis of self-phase-locking with the benefit of an extended (optical) servo bandwidth. The potential of this 3-to-1 device for generating dissipative spatiotemporal structures has been recently suggested [15]. The phase-invariance breaking due to self-phase-locking, combined with diffraction, spatially lifts the plane-wave phase degeneracy, leading to the formation of three-phase-encoded spiraling transverse intensity patterns. Future investigation of the quantum aspects of the 3-to-1 SPL-OPOs may lead to potential application in quantum information technology, such as ultrastable continuous-variable quantum entanglement [3,4] and multipartite entanglement based on competing nonlinearities [7].

F. Wong acknowledges the support of the DoD MURI Program administered by ONR under Grant No. N00014-02-1-0717.

*Electronic address: jean-jacques.zondy@obspm.fr

†Permanent address: Institute of Laser Physics, Novosibirsk, Russia.

- [1] C. D. Nabors *et al.*, J. Opt. Soc. Am. B **7**, 815 (1990).
- [2] E. J. Mason and N. C. Wong, Opt. Lett. **23**, 1733 (1998).
- [3] H. H. Adamyán and G. Yu. Kryuchkyan, Phys. Rev. A **69**, 053814 (2004).
- [4] J. Laurat *et al.*, quant-ph/0403224.
- [5] G. Izús *et al.*, Phys. Rev. E **64**, 056231 (2001).
- [6] D.-H. Lee *et al.*, Phys. Rev. A **67**, 013808 (2003).
- [7] O. Pfister *et al.*, quant-ph/0404049 [Phys. Rev. A (to be published)].
- [8] J.-J. Zondy *et al.*, Phys. Rev. A **63**, 023814 (2001).
- [9] J.-J. Zondy, Phys. Rev. A **67**, 035801 (2003).
- [10] L. A. Lugiato *et al.*, Nuovo Cimento D **10**, 959 (1988).
- [11] M. Bache *et al.*, Phys. Rev. A **65**, 033811 (2002).
- [12] L. E. Meyers *et al.*, J. Opt. Soc. Am. B **12**, 2102 (1995).
- [13] A. Douillet *et al.*, IEEE Trans. Instrum. Meas. **50**, 548 (2001).
- [14] A. Douillet *et al.*, J. Opt. Soc. Am. B **16**, 1481 (1999).
- [15] S. Longhi, Phys. Rev. E **63**, 055202 (2001).